



Radiation Spectral Analysis of 3D Dust Molecular Clusters (PAHs) and Peptoids under Ionization and Electric Field in ISM

Ruiqing Wu¹, Chunhua Zhu², Guoliang Lü², Xiaojiao Zhang³, Xizhen Lu², Jinlong Yu⁴, Wujin Chen⁵, and Mengqiu Long¹

¹School of Physics and Electronics, Central South University, Changsha 410083, China; ruiqingwu163@163.com, mqlong@csu.edu.cn

²School of Physical Science and Technology, Xinjiang University, Urumqi 830046, China

³School of Microelectronics and Physics, Hunan University of Technology and Business, Changsha 410205, China

⁴College of Mechanical and Electronic Engineering, Tarim University, Alar 843300, China

⁵School of Medicine, Xinjiang Medical University, Urumqi 830011, China

Received 2023 August 7; revised 2023 October 13; accepted 2023 October 20; published 2023 December 12

Abstract

Polycyclic aromatic hydrocarbons (PAHs), PANHs, and peptoids dust spectral calculations from the interstellar medium (ISM) are important for dust observations and theory. Our goal is to calculate the radiation spectrum of spherical PAHs dust clusters in a vacuum containing ionized and applied in the presence of an electric field. We propose a new simple computational model to calculate the size of three-dimensional spherical dust clusters formed by different initial dust structures. By the Vienna Ab-initio Simulation Package code, the density functional theory with the generalized approximation was used to calculate the electron density gradient and obtain the radiation spectrum of dust. When the radius of spherical dust clusters is $\sim[0.009\text{--}0.042]$ μm , the dust radiation spectrum agrees well with the $Z=0.02$ mMMP stellar spectra, and the PAHs radiation spectrum of NGC 4676 at wavelengths of $(0\text{--}5)$ μm and $(5\text{--}10)$ μm , respectively. In the ionized state, the N-PAH, $\text{C}_{10}\text{H}_9\text{N}$, $2(\text{C}_4\text{H}_4)^{1+}$, and peptoids $4(\text{CHON})$, $(\text{C}_8\text{H}_{10}\text{N}_2\text{O}_5)^{1+}$ dust clusters at 3.3 μm , while the $2(\text{C}_{22}\text{H}_{21}\text{N}_3\text{O}_2)^{1+}$, $4(\text{CHON})$ dust clusters at 5.2 μm have obvious peaks. There is a characteristic of part of PAHs and peptoids clusters radiation at the near-infrared wavelength of 2 μm . However, especially after applying an electric field to the dust, the emission spectrum of the dust increases significantly in the radiation wavelength range $[3\text{--}10]$ μm . Consequently, the dust clusters of PAHs, PANHs, and peptoids of the radius size $\sim[0.009\text{--}0.042]$ μm are likely to exist in the ISM.

Key words: ISM: structure – ISM: molecules – radiation mechanisms: general – (ISM:) dust – extinction

1. Introduction

Polycyclic aromatic hydrocarbons (PAHs) molecules in the interstellar medium (ISM) always contain two or more fused benzene rings, which also include other types of functional derivatives such as N-PAH, and O-PAH, they are mainly composed of ^1H , ^{12}C , ^{14}N , and ^{16}O four elements Silva-Ribeiro et al. (2022). It has been shown that the PAHs play a crucial role in the ionization and energy balance of the ISM in galaxies (Sellgren 1984; Genzel et al. 1998). This has attracted wide interest currently, particularly since Li et al. (2014) detected for the first time the peptide molecule propionamide ($\text{C}_2\text{H}_5\text{CONH}_2$) from the space of Sagittarius B2(N1).

In general, the PAHs are an important component of cosmic dust, dust originates from the stellar winds of the asymptotic giant branch (AGB) and supernova remnant (SNR), as well as in novae ejecta in astrophysical theoretical studies. During the post-asymptotic giant branch (post-AGB) stellar period, traces of PAHs can be found in the stellar spectrum as the stellar temperature increases. The reason is that PAHs require energy provided by ultraviolet (UV) or optical radiation to support their radiation energy to form the infrared spectrum

(Tielens 2008; Zhu et al. 2013; Sarangi et al. 2018; Duolikun et al. 2019; Marassi et al. 2019; Zhu et al. 2019; Rho et al. 2021; Wu et al. 2021; Cinquegrana & Karakas 2022).

PAHs are frequently observed in astrophysical environments, including the Milky Way (MW), Seyferts, and Starbursts galaxies (Brandl et al. 2006; Smith et al. 2007; Sales et al. 2010; Draine et al. 2021). Moreover, PAHs also show that obvious emission characteristics at wavelength 3.3 , 5.25 , 5.7 , 6.0 , 6.2 , 6.7 , 7.4 , 8.3 , 8.6 , 10.5 , 11.0 , 12.0 , 13.6 , 14.2 , 15.8 , 16.4 , 17.4 and 17.8 μm (Allamandola et al. 1989; Peeters et al. 2004; Smith et al. 2007; Tielens 2008; Li 2020; Silva-Ribeiro et al. 2022). Furthermore, interstellar dust affects the appearance of galaxies by attenuating short-wavelength radiation from stars and ionized gas, and emitting in infrared (IR) and far-infrared (FIR) band, even in the near-infrared (NIR) band. In the observed infrared band, there are some Unidentified Infrared Emission (UIE) features in the nebula observed spectrum. For example, 3.3 and ~ 2 μm in the reflection nebula NGC 2023 in recent decades have no definite physical separation and chemical carrier certification (Duley 1976; An & Sellgren 2003; Draine 2003).

Joham & Dorfi (2012), and Hanine et al. (2020) suggested that the Onion–Like (3D Spherical) nano-structures in the ISM are likely to grow through Layer–By–Layer adsorption and evolution. In this article, we do not calculate the chemical reaction and the process of dust structure growth. But we calculated results by the initial unit radiation spectrum showing that the precise size of dust was in the range of $\sim(4.5 \text{ \AA}–0.4) \mu\text{m}$ (Todini & Ferrara 2001; Draine et al. 2021). In diffuse ISM, massive amounts of dust are exposed to a wider range of photon energies, and the photoelectric charging could play a significant role in the radiation-stable growth of large dust particles, and complex physical interactions between photons and electrons and radiation fields may diversify charged PAHs (Siebenmorgen et al. 2014; Murga et al. 2019). The photodissociation regions (PDRs) of the central star will lead to a large number of escaping photons when the dust is irradiated. If the absorption rate of photons by the dust structure exceeds the numerical value of the collision rate between electrons and various surrounding particles, the photoelectric charging induces the particles to be positively charged (Draine 2011). Dust is often lit up by photons from gamma-ray bursts or active galactic nuclei. At the same time, dust is prone to cause Coulomb explosions accompanied by the heating of electric charges by high-energy photons (Waxman & Draine 2000; Tazaki et al. 2020). In areas near the PDR, the large PAHs are more likely to be ionized and will reach a dicationic state (Tielens 2005; Andrews et al. 2016). The charge of dust and surface (de)hydrogenation reactions can also affect the optical absorption spectra (Cecchi-Pestellini et al. 2008, Mallocci et al. 2008) and radiation spectra of PAHs. The intensity of the radiation spectrum depends on the electromagnetic energy density and emissivity, which are intrinsic characteristics of material, and the inherent characteristics of temperature size (Brar et al. 2015).

Marciniak et al. (2015) and Wenzel et al. (2020) have investigated the range of photon energies that exist in the H_{II} region and the ionization front Interaction of PAHs cations with UV photons within [9–20] eV. (Paul & Grinberg 2022) studied the electro-optic coefficients as a function of photon energy for MoS_2 , MoSe_2 , WS_2 , and WSe_2 , in which photon energies ranged from [0.25 to 4] eV. Even the electric field can cause band-valley splitting and discontinuous changes in the structure of two-dimensional materials (Yin et al. 2022). Dust particles immersed in a low-density plasma with a direct current or radio frequency discharge acquire a large negative charge. When an external electric field breaks the spherical symmetry of the plasma distribution around the dust particles, the system of negatively charged dust particles and positive ion clouds is polarized and acquires a dipole moment (formation of a “dust quasi-atom”). A Monte Carlo simulation study of the polarization of the plasma around dust particles in an external electric field has been carried out by Sukhinin et al. (2012).

In recent years, many research groups have studied the dust and heavy elements (^1H , ^{12}C , ^{13}C , ^{14}N , ^{15}N , and ^{16}O) yield of AGB stars (Ferrarotti & Gail 2006; Karakas & Lattanzio 2007; Ventura et al. 2020, 2021; Cinquegrana & Karakas 2022). Until now, only a few groups have studied the PAHs dust of ISM and the relationship between the size of dust and the radiation spectrum. It has important research significance to uncover the underlying physical relationships, not only three-dimensional (3D) globular cluster, and size, but also the radiation spectrum of ionized dust, and the comparative analysis of its radiation spectrum, stellar spectrum, and there are even PAHs radiation characteristics. The study of the content and structure and shape of PAH has a deeper role and impact. For the purpose of studying the effect of photon energy on the dust radiation spectrum, we consider the electric field forces for different electric fields at low-photon energies of 4 and 20 eV \AA^{-1} . Since the temperature of PAHs dust formation is low to 25 K (Dartois et al. 2017), this effect will be ignored in this article. The topic of PAHs, PANHs, and peptoids dust yield is especially important and fascinating, because we can better understand the origin of PAHs and the basic laws of stars, the evolution of ISM, and the extinction of dust on the observation. In Section 2, the physical parameters of the model used are outlined. Detailed results are discussed in Section 3. The conclusions are drawn in Section 4.

2. Models and Methods

The physical parameters of Viaing Vienna Ab–initio Simulation Package (VASP) are set as follows: the energy convergence of the standard is 1×10^{-6} eV, the Hellmann–Feynman forces of the standard are set to $\leq 1 \times 10^{-2}$ eV \AA^{-1} , and the vacuum layer is [20–25] \AA along the z -direction (Zhang et al. 2018; Wu et al. 2022). The lattice angles of each dust structure are $\alpha = \beta = \gamma = 90^\circ$. In these structural calculations, the purpose of the vacuum layer is to prevent the dust structure from interacting with other unit structures. The Brillouin zone integration is performed using the $1 \times 1 \times 1$ for static calculation. The calculation is performed by the Kohn–Sham equation iteration method and the projected wave plane wave pseudopotentials focus on density functional theory (DFT) (Kohn & Sham 1965). Here, the structural optimization and the corresponding calculation of the optical spectrum are mainly performed using the Perdew–Burke–Ernzerhof (PBE) function of the exchange-dependent generalized gradient function, and the final plane wave cutoff energy is equal to 400 eV (Rani et al. 2014; Lin et al. 2016; Yao et al. 2021).

The optical spectrum of dust can be calculated from the complex dielectric function:

$$\varepsilon(\omega) = \varepsilon_1(\omega) + i\varepsilon_2(\omega), \quad (1)$$

where $\varepsilon_1(\omega)$ and $\varepsilon_2(\omega)$ are the real and imaginary parts of the dielectric function, they are a function of photon frequency (ω).

The absorption strength $\alpha(\omega)$ is as follows:

$$\alpha(\omega) = \frac{\sqrt{2}\omega}{c} [\sqrt{\varepsilon_1(\omega)^2 + \varepsilon_2(\omega)^2} - \varepsilon_1]^{1/2}, \quad (2)$$

here, c is the speed of light. We assume that the reflectivity of smooth dust is approximately equal to the emissivity of dust, because the vibrational frequency of electrons around dust atoms does not match the frequency of light waves. When an atom or molecule in an excited state transition back to the ground or lower excited state, the energy is emitted in the form of new light waves radiation, forming an emission phenomenon (Nagasaka et al. 2005; Yin et al. 2006; Orszagh et al. 2022; Takahashi et al. 2022). The reflectivity of dust is close to 1.

The emission strength $E(\omega)$ is calculated by this formula:

$$E(\omega) = \frac{(n-1)^2 + K^2}{(n+1)^2 + K^2}, \quad (3)$$

where n and K are the real and imaginary parts of the emission index, respectively. The use of the ionization state parameter for dust relies on the arbitrary loss of [1–2] electrons from the total number of electrons (Rani et al. 2014; Wang et al. 2016; Yao et al. 2021; Wu et al. 2022). In the presence of an electric field, the parameter IDIPOL turns on monopole/dipole and quadrupole corrections for total energy. In the calculation of VASP, the parameter IDIPOL = 4 is to obtain the full dipole moment in all directions (refer to 1). The dipoles are enabled to perform monopole corrections on the potentials, enabling a potential reset of the local potentials, and finally correcting for errors introduced by periodic boundary conditions (Neugebauer & Scheffler 1992).

In the vinylacetylene (C_4H_4) molecule model, the optimized lattice constant is calculated as $a = b = c = 3.277 \text{ \AA}$, the optimized H–C bond length is (1.07–1.09) \AA , the optimized C–C bond length is (1.47–1.49) \AA , which are consistent with the results of McMullan et al. (1992), Pereira et al. (2020). C_4H_4 is a chemical reaction product of C_2H_2 , and C_2H_2 has been detected in the spectra of three IR sources embedded in molecular clouds, C_4H_4 is one of five molecules detected after Fourier transform infrared spectroscopy (FTIR) analysis by irradiation of acetylene ice (Lacy et al. 1989; Abplanalp & Kaiser 2020). It is necessary to study the relevant structural optical properties of this second structure.

In addition, the cohesive energy of dust is primarily obtained by the following formula:

$$E_{\text{coh}} = (nE_h + mE_c - E_{\text{tot}})/(n + m), \quad (4)$$

where, E_h , E_c , and E_{tot} are the energy of a single ^1H atom, ^{12}C atom, and total energy of the monolayer structure C_4H_4 , respectively. These physical parameters n and m are the numbers of ^1H and ^{12}C atoms in the monolayer structure, respectively. The calculated cohesive energy per atom of

(C_4H_4) is 5.73 eV. This is close to the C–H bond energy of Abplanalp & Kaiser (2020) 5.7 eV. Be_5C_2 (per atom 4.58 eV), and Be_2C (per atom 4.86 eV) (Li et al. 2014; Wang et al. 2016; Fan et al. 2020). Therefore, such a high cohesion can keep the C_4H_4 structure as a stability connection network. The molecular structure C_4H_4 is regarded as a stable molecular structure after structural optimization.

We choose these stable and well-optimized initial structures as follows: $C_{36}H_{16}$, and $C_{10}H_9N$ (refers to models of Silva-Ribeiro et al. 2022), the two components accounted for 4.9 and 6.8 percent of the total content of PAHs in the NGC 4676, respectively. They are derived from the structure of Haley et al. (1997), Bond (2010), respectively. The 4(CHNO) is an isomer of isocyanic acid (HNCO) that has been detected in the ISM (Beltrán et al. 2018). The structure of the peptoid small molecule 4(CHNO) is established according to the structure of Worsham et al. (1957), and the rest structures $C_8H_{10}N_2O_5$, $C_{22}H_{21}N_3O_2$, and $C_{24}H_{38}O_5$ are from the models of Bouchouit et al. (2004), and Hossain et al. (2020) and Tang et al. (2019), respectively. $C_8H_{10}N_2O_5$ also contains the peptide-like bond and NH_2 , $\text{H}_2\text{NC}_2\text{O}$, NH_4^+ , and NC_2O^{1-} . The $C_{24}H_{38}O_5$ PAHs structure is compared with the peptoid structures. Astronomical observations in the 1960s of last century found that throughout cosmic space (including the vacuum) there is always 3K microwave background radiation Jagannathan et al. (2021). Gravitational and electromagnetic fields Babich et al. (2007) (including radio waves, microwaves, infrared light, visible light, ultraviolet light, and gamma-rays Porter et al. 2017) like this one exist in the universe. An electron meeting a positron will annihilate and be converted into a photon, i.e., into an electromagnetic field. In the nuclear field photon energy is large enough, photons can be converted into pairs of positive and negative electrons, electrons and positrons are physical objects, while photons are electromagnetic fields, that is, the vacuum. We consider the electrostatic field, that is, the electrostatic field is applied to different charge sizes. The electrostatic field refers to the electric field observed when the observer is at rest relative to the charge. The electrostatic field in the “static,” is the absolute static and relative static two layers of meaning, absolute static is the observer and the charge carried by the study of the charge does not change with time, and relative static is the study of the charge and the observer to remain relatively static. Obviously we use a relatively stationary electric field, which regulates the magnitude of the photon and the magnitude of the electromagnetic field. Based on the fact that the cationic and electronic actions of the nanoparticles dominate the main reactions, ignoring the actions of other fields, so here we assume that the electrostatic field is equivalent to the harmonic field of the cosmic radiation field at the nanoscale.

1. <https://vasp.at/wiki/index.php/The-VASP-Manual>.

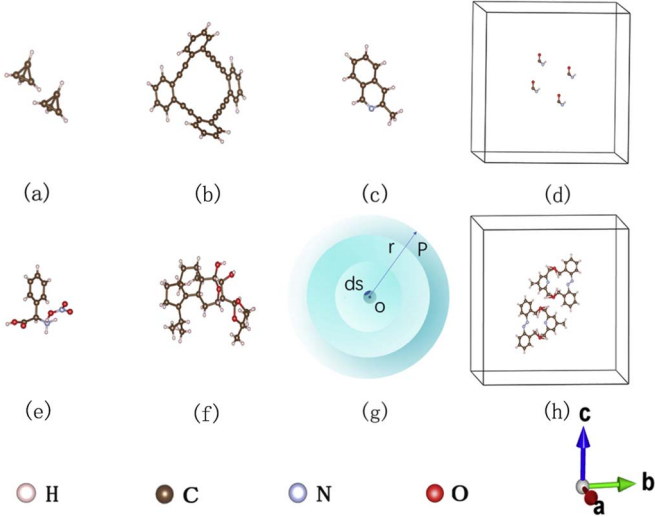


Figure 1. Subgraphs (a) and (b) are the structural models $2(C_4H_4)$ (2 represents two C_4H_4 molecules) and $C_{36}H_{16}$, subgraph (c) is the structural models of N-PAH, $C_{10}H_9N$, subgraphs (d), (e) are the structures of peptoids (PANO), 4(CHNO), $C_8H_{10}N_2O_5$, respectively. Subgraph (f) is the structural models of O-PAH, $C_{24}H_{38}O_5$, subgraph (g) is a model figure of 3D spherical clusters of dust. Subgraph (h) is the structure of peptoids (PANO), $2(C_{22}H_{21}N_3O_2)$.

3. Results

Our results show that the size of the dust clusters with the applied electric field is smaller than that of the unemployed in the presence of an electric field, while their radiation spectra are substantially consistent with those of stars. Moreover, the spectra of 3D dust are consistent with those of mmMp stars, and PAHs in NGC 4676 in the band range of (0–10] μm . Dust clusters have prominent peaks especially at radiative wavelengths 2, 3.3, 5.2, and 6.2 μm , which correspond to the radiation peaks 5.2 and 6.2 μm of PAHs on the astronomically observed spectrum.

3.1. Ionized Spherical Clusters of Dust

Ions interact with surrounding gases, ambient radiation fields (like absorption and photoelectron emission), and other particles (like condensation). These physical reaction processes usually result in the dust acquiring non-zero charges, which in turn strongly affect subsequent interactions (e.g., Draine 2011). On the surface of stars associated with these photodissociation regions (PDRs), for PAHs cations, fragmentation was observed to be the dominant channel, associated with the H_I region at a photon energy of 13.6 eV, the channels generated by PAHs cations are expected to be primarily ionization (Tielens 2005; Andrews et al. 2016; Zhen et al. 2016).

In Figure 1, we plotted the ideal dust growth as a spherical cluster and ignore intermolecular chemical reactions and bond length changes, and assumed that the forming way of the dust clusters form is a spherical growth Layer-By-Layer by referring

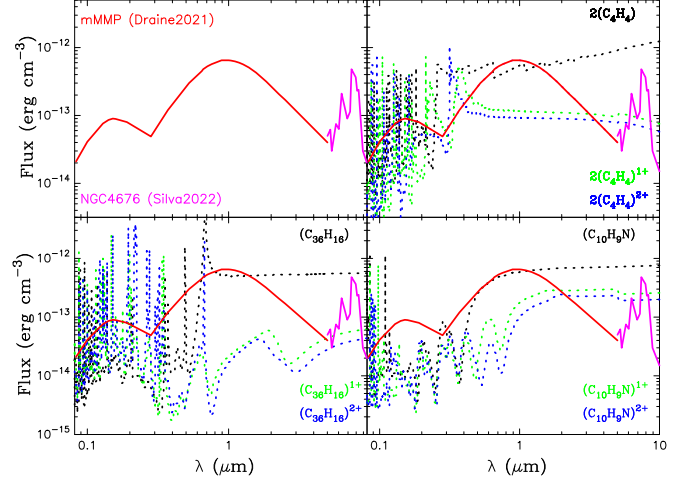


Figure 2. The radiation spectrum of molecular and PAHs dust clusters is shown, and the change of the radiation spectrum of dust clusters in the ionized state is considered. The red dotted line in the figure represents the fitted mMMP stellar radiation spectrum of Draine et al. (2021). The unionized state of the dust structure in the annotation is 0+, the others 1+, and 2+ valence represents the ionized state.

to the work of Hanine et al. (2020). As shown in Subgraph (g), the central core is the first a small cluster of dust, and we took the unit area element as our initial molecules C_4H_4 of the dust clusters, or one of the other six structures, and the center point O to point P is the radius of the dust clusters (r_d).

In Figure 2, the radiation intensity of spherical clusters (F_v) is calculated by the following formula:

$$F_v = \int_0^{r_d} F_i 4\pi r^2 dr, \quad (5)$$

where F_i is the radiation intensity per unit of initial molecular structure, which is obtained by the radiation intensity calculation of Kirchhoff (1860),

$$\frac{E}{\alpha} = F_i, \quad (6)$$

here, E and α are the emission intensity and absorption intensity, respectively. The radiant intensity of dust is the flux of radiation produced by the light of a central star that penetrates the dust (Wu et al. 2022). Table 1 shows the surface area of the unit structure (ds) and final radius (r_d) of the dust clusters of seven initial structures, and radiation losses are not considered in this article. The r_d refers to the final size of the dust when it grows to the same size as the 3D structure and the stellar spectrum. The r_E also refers to the final size when the electric field is applied to grow to the same size as the stellar spectrum.

At the same time, Figures 2 and 3 show the radiation spectra of seven kinds of spherical dust clusters are close to the stellar spectra mMMP of the MW fitted by Draine et al. (2021), which means that the MW may exist in such dust structures. In

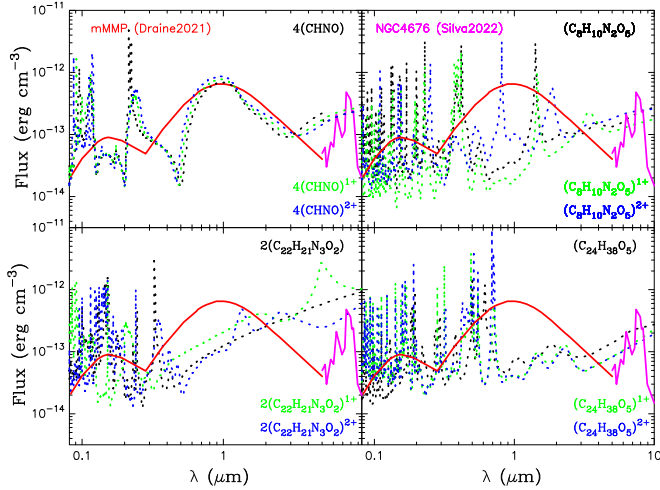


Figure 3. The curve is the radiation spectrum of PANOH dust clusters, and the change of the radiation spectrum of dust clusters in the ionized state is considered. The magenta dotted line represents the observed spectrum of NGC 4676 fitted with pahdb code in the work of Silva-Ribeiro et al. (2022).

Table 1

The Surface Area of the Unit Structure (ds) and the Final Radius of Spherical Dust Clusters

Initial Structure	ds/(Å ²)	r _a /(μm)	r _E /(μm)
2(C ₄ H ₄)	10.43	0.039	0.009
C ₃₆ H ₁₆	38.57	0.037	0.031
C ₁₀ H ₉ N	35.30	0.040	0.031
4(CHNO)	103.80	0.024	0.024
C ₈ H ₁₀ N ₂ O ₅	26.13	0.042	0.031
2(C ₂₂ H ₂₁ N ₃ O ₂)	213.02	0.032	0.031
C ₂₄ H ₃₈ O ₅	97.71	0.031	0.031

Figure 2, the PAHs radiation spectrum and the fitted stellar spectrum are more consistent with the PAHs neutral structure are 2(C₄H₄) and (C₁₀H₉N) in the near-infrared band [0.5–1.5] μm. The 1+ valence or 2+ valence structure has a somewhat lower radiation spectrum than the neutral structure owing to its absorption spectrum being about an order of magnitude higher (see Figure 4).

In Figure 3 of peptoids dust, it is the opposite of the former result, that is the radiation spectrum of the cationic structure is higher than that of the neutral structure. The reason would be that the peptoid structure (C₈H₁₀N₂O₅) takes into account that the radiation of the ionizing structure is weaker compared to the radiation spectrum of the neutral structure (see Figure 4). Among them, the 4(CHNO), C₈H₁₀N₂O₅, and 2(C₂₂H₂₁N₃O₂) structures are well consistent with the mMMP star spectrum in the near-infrared band of [0.5–10] μm. It is particularly important that the 2(C₄H₄)¹⁺, (C₈H₁₀N₂O₅)¹⁺, and 4(CHON) structures have a peak at 3.3 μm, and 4(CHON) has a peak at 4.4 μm. The 3.3 μm PAHs emissions also have been detected

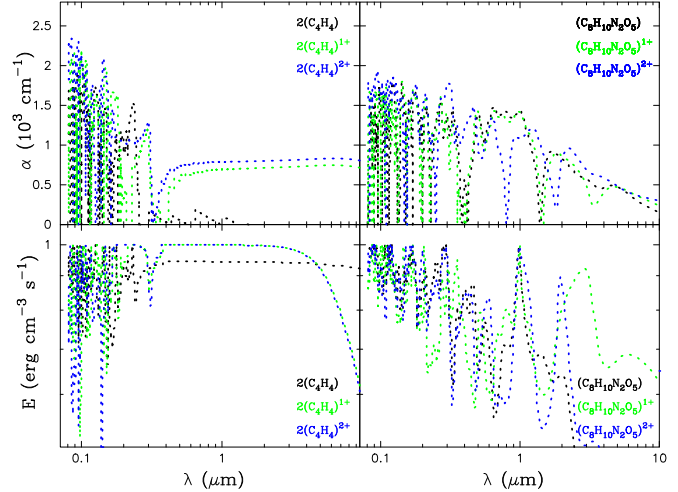


Figure 4. 2(C₄H₄) and C₈H₁₀N₂O₅ dust absorption and emission spectra are shown in the upper and lower panels, respectively.

in the NIR spectrum of M82 by Yamagishi et al. (2012). van Broekhuizen et al. (2004) pointed out that the IR data obtained from reflection experiments indicated that the structure had a strong radiation peak at 4.41 μm. Lattanzi et al. (2015) observed microwave and millimeter–wave rotational spectra of NCO^{1−} in a supersonic beam using a Fourier transform (FT) microwave spectrometer, its peak value is also precisely at 3.3 μm (McCarthy et al. 2000).

Moreover, 2(C₂₂H₂₁N₃O₂)¹⁺ and 4(CHNO) have a peak at 5.2 μm close to Spitzer/IRS observes a minor signature of PAHs at 5.25 μm (e.g., Peeters et al. 2004; Smith et al. 2007; Tielens 2008).

Here, the curve of the observed spectrum of NGC 4676 is obtained after this processing, its original radiation intensity is multiplied by 3×10^{-15} . Obviously, most of the peptoid structures in the figure pass through the observed spectrum of NGC 4676 of Silva-Ribeiro et al. (2022), with weak peaks corresponding to wavelengths of 6.2 and 7.4 μm. Silva-Ribeiro et al. (2022) also show that 65.3 percent of the other heteroatomic dust spectrum is in NGC 4676. According to the effect of peptoid 4(CHNO) radiation intensity, we can well explain the phenomenon that observing the radiation spectrum of PAHs dust is higher than the theoretical value, since these peptoid heteroatomic radiation spectra may also exist in NGC 4676, although they are often not easily observed by researchers. We have chosen the absorption and emission spectra of two types of dust to display, as above 2(C₄H₄) and C₈H₁₀N₂O₅ in Figure 4. Finally, we can see that the radiation spectrum of PAHs dust in the ionized state has prominent peaks at near-infrared wavelengths 0.6, 0.65, 0.8, 1.0, 1.5, 1.8, 2.0, and 2.5 μm and a large number of near-infrared PAHs and peptoids radiation eigenvalues have not been verified by current observations.

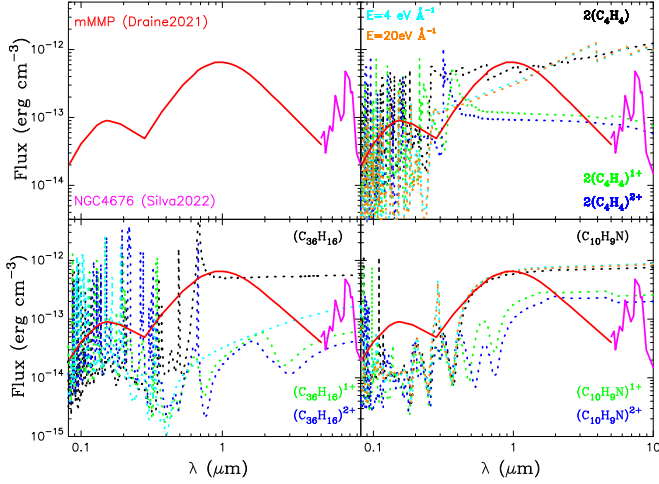


Figure 5. Radiation spectrum showing applied electric field for PAHs dust clusters, and the change of the radiation spectrum of dust in the ionized state is considered. In addition, two electric fields are considered in the model, the light blue and orange colors represent the electric force fields of 4 and 20 $\text{eV} \text{ \AA}^{-1}$, respectively.

3.2. Comparison of Spherical Dust Clusters in Ionized State and in the Presence of Electric Field

Inside the molecular cloud is shielded from UV radiation. Dust is highly penetrated by X-rays/cosmic rays and their secondary products and their charge will also change (Ivlev et al. 2015). Photoionization is the study of grain charging and provides the basis for models of galaxy formation, due to the fact that it involves radiation fields and gas ionization (Ferland et al. 2017; van Hoof et al. 2020; Glatzle et al. 2022). Obviously, the radiation field in the interstellar environment will also have a certain effect on the optical properties of the dust, such as the emission coefficient and absorption coefficient. The following is to explore the effect of an electric field on the radiation spectrum of dust. Most importantly, we compared spherical dust clusters in the ionized state and in the presence of an electric field.

In Figure 5, we can see that the radiation spectra of the two electric force fields of the $\text{C}_{36}\text{H}_{16}$ models overlapped, and both are represented by the light blue line. (C_4H_4) , $(\text{C}_{36}\text{H}_{16})$, and $(\text{C}_{10}\text{H}_9\text{N})^{2+}$ models have a distinct characteristic peak at wavelength $2 \mu\text{m}$. As shown in Table 1, it is clear that the radius of the dust cluster is constantly changing with the applied electric field function. Most of them show a decreasing trend. First of all, the radius of the spherical clusters of dust to which the electric field is applied becomes smaller when both the dust radiation spectrum is close to the radiation spectrum of mMMP stars (see Table 1, parameter r_E is the final radius of the dust cluster after applying an electric field). Only when the radii of the two structures ($4(\text{CHNO})$, $\text{C}_{24}\text{H}_{38}\text{O}_5$) with r_d and r_E radii of 0.024 and 0.031, respectively, were unchanged, the rest of

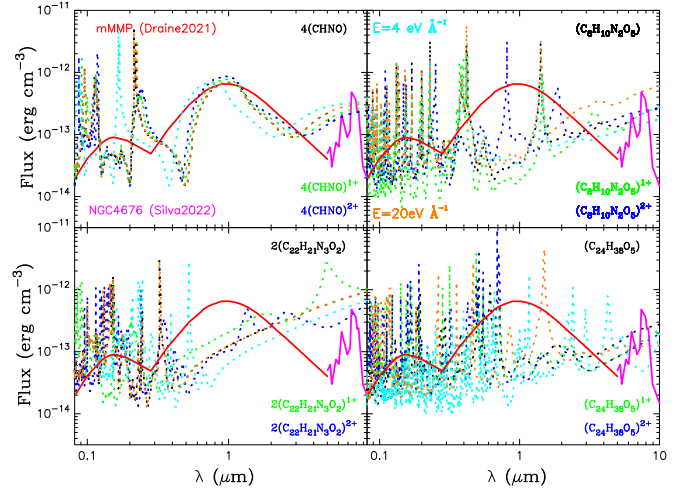


Figure 6. Radiation spectrum showing the applied electric field for PANOH dust clusters, and the change of the radiation spectrum of dust in the ionized state and electric fields are considered.

the structures showed a decrease in radius after the electric field was applied. On account the emission spectrum of electric field dust is higher than that of ionized dust, it is more obvious when the wavelength range is $[3-10] \mu\text{m}$, as shown in Figure 7. Second, the $2(\text{C}_4\text{H}_4)$ model is very close to the peaks 6.2, and $8.6 \mu\text{m}$ observed by PAHs when the wavelengths are 6.2 and $8.9 \mu\text{m}$, under the action of the electric force field 4 and $20 \text{ eV} \text{ \AA}^{-1}$. These PAHs models consider electric fields all have higher radiation spectra than PAHs cations and are very close to neutral PAHs. Third, with the increase of the electric field force field, the radiation spectrum is slightly weakened but the change is not obvious.

In Figure 6, the change in the size of the radiation spectrum of the PANOH dust clusters after applying an electric field is consistent with that of PAHs. The radiation spectrum of the $4(\text{CHNO})$ model with the electric field and the radiation spectrum of the model considering the ionization state are in good agreement with the spectrum of the star in the wavelength range $(0-10) \mu\text{m}$. Therefore, there is also a great probability that a large number of clusters composed of peptoids small molecules exist in the local galaxy. Model $(\text{C}_8\text{H}_{10}\text{N}_2\text{O}_5)^{1+}$ takes into account the radiation spectrum of the electric field with peaks at wavelength $3.3 \mu\text{m}$, $(\text{C}_8\text{H}_{10}\text{N}_2\text{O}_5)$, $2(\text{C}_{22}\text{H}_{21}\text{N}_3\text{O}_2)^{1+}$, and $(\text{C}_{24}\text{H}_{38}\text{O}_5)^{2+}$ models have a characteristic peak at wavelengths $2 \mu\text{m}$. Model 2 ($\text{C}_{22}\text{H}_{21}\text{N}_3\text{O}_2$) has peaks at 0.5, $0.7 \mu\text{m}$, and model $\text{C}_{24}\text{H}_{38}\text{O}_5$ has the most peaks, including wavelengths in the range $[0.5-1.5] \mu\text{m}$, and wavelengths of 2.2, 2.8, 4.1, and $5.2 \mu\text{m}$. All the above peptoid models have many peaks in the ultraviolet and visible wavelengths and are in good agreement with the stellar spectrum. The relationship between the electric field magnitude and the radiation spectrum is consistent with the third point of the above PAHs.

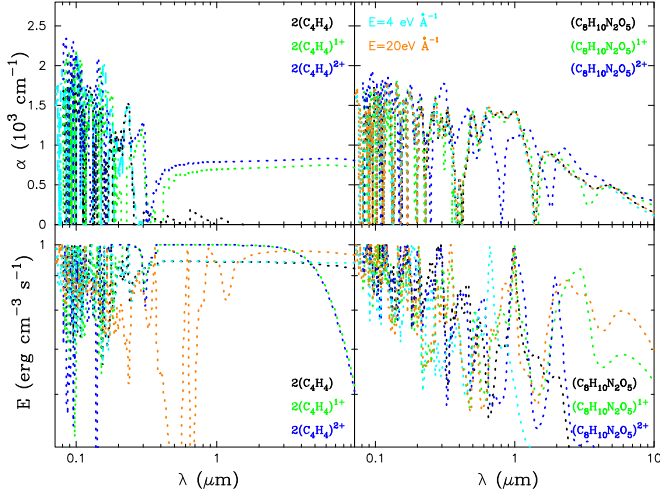


Figure 7. We compare $2(\text{C}_4\text{H}_4)$ and $\text{C}_8\text{H}_{10}\text{N}_2\text{O}_5$ in absorption and emission spectra of ionized and in the presence of electric field.

In Figure 7, the spectrum of the selected two types of dust increases after the electric force field is applied, while the change in the absorption spectrum of dust is weaker, the latter results are very similar to the work of Paul & Grinberg (2022) calculated MoSe_2 material. Therefore, the radiation spectrum of the dust per unit structure increases. With the increase of the electric field force, the emission spectrum increases more significantly. After applying the electric field, the atoms and electrons gain energy to generate induced polarization to vibrate at a certain frequency, forming a vibrating electric dipole, which radiates to the ISM again in the form of light waves. We find that the dipole moment of dust does not change obviously with the increase of electric field force (the change of total electronic dipole moment is in the range of $[0.001\text{--}0.002] e \cdot \text{\AA}$). The change of total energy will be weakened with the increase of electric field force. In fact, the dipole moment does not change much with the electric field, however, it is very related to the distance between the positive and negative electron pairs. The smaller the distance the smaller the dipole moment. Moreover, considering that the main reason for the difference in the radiation spectra of cations and uncharged particles is the difference in the number of charges, we make the total number of charges of the molecule randomly minus one electron to get a positively monovalent cation, and similarly minus two electrons to get a positively divalent cation. When a molecule containing the element H, C, and PAHN loses electrons, its absorption coefficient increases, and when the emission coefficient changes, the intensity of radiation increases. For peptide molecules containing H, C, N, O the opposite is true. According to the definition of plasma: plasma is an ionized gas-like substance composed of positive and negative ions generated by the ionization of atoms and atomic groups after losing some electrons. The macroscopic

scale of the electroneutral ionized gases is larger than the length of the débay, whose motions are mainly governed by the electromagnetic force and which exhibit remarkable collective behavior. The plasma is widespread in the universe, including ionized gas-like materials. Sukhinin et al. (2012) studies of the ion trajectories of plasma dust particles applied electric fields show that larger dipole moments have a non-monotonic relationship with the applied electric field. However, for very small electric fields, its dependence on the charge of the dust particles is weak.

Hence, it can be explained that the dust clusters formed are smaller than the dust that does not apply an electric field and considers the ionized state, which can provide a similar radiation intensity as that without an electric field. This also shows from the side that the electric field has a certain inhibitory effect on the increase of the dust cluster size, when we assume that it is the same as the radiation intensity without the electric field being applied. We calculated to obtain a final growth size and thus determine the maximum value of the dust cluster. It is clear that the radius of the applied electric field obtained for different structures is smaller than the radius of the unapplied electric field, so we believe that the electric field has a suppressive effect on the radius growth of the dust clusters.

Although the dust structure of 2, 3.3 μm and more radiation eigenvalues have almost no observational verification, we expect the James Webb Space Telescope (JWST) and the upcoming Chinese Space Station Optical Survey Telescope (CSST) to achieve breakthroughs in the near-infrared spectrometer (NIRSpec) working band of $(0.6\text{--}5) \mu\text{m}$, and hope that this work can provide a theoretical basis for the observation of dust clusters.

4. Conclusions

We calculated the radiation spectra of PAHs and peptoids dust clusters in the ionized state and under an applied electric field, and compared these results with the observed mmMp stars and the NGC 4676 radiation spectra. There is a characteristic of PAHs and peptoids radiation at the near-infrared wavelength of $2 \mu\text{m}$, $3.3 \mu\text{m}$, and the PAHs and peptoids dust clusters structure in the ionized state and neutral structure $2(\text{C}_4\text{H}_4)^{1+}$, and $(\text{C}_8\text{H}_{10}\text{N}_2\text{O}_5)^{1+}$ have an obvious peak. $4(\text{CHON})$ has a peak at $4.4 \mu\text{m}$, $2(\text{C}_{22}\text{H}_{21}\text{N}_3\text{O}_2)^{1+}$ and $4(\text{CHON})$ at $5.2 \mu\text{m}$ have an obvious peak.

The emission and radiation spectrum of the dust increased significantly after applying the electric field, while the absorption spectrum remained basically stable. The $(\text{C}_8\text{H}_{10}\text{N}_2\text{O}_5)$ model has a peak at wavelength $3.3 \mu\text{m}$. The $\text{C}_{24}\text{H}_{38}\text{O}_5$ model corresponds to the peaks of the optical PAHs at wavelength $2.2 \mu\text{m}$, $2.8 \mu\text{m}$, $4.1 \mu\text{m}$, and $5.2 \mu\text{m}$. Clearly, the peptoid clusters are more sensitive to the electric field than the radiation spectrum of dust clusters considering ionized states. These results suggest that PAHs and peptoid structures

are likely to occur near stars in the local galaxy, as well as in NGC 4676 galaxies. Whereas, dust with an electric field radiation spectrum is higher than the spectrum of ionized dust. In the ultraviolet and visible light bands with wavelengths of [0.08–0.7] μm , and infrared band [0.7–10] μm , the above dust models have outstanding contributions, which fit well with the radiation spectrum of mMMP stars or from the observed spectrum NGC 4676. We believe that PAHs and peptoid dust are likely to originate from stars in the local galaxy and NGC 4676.

The size of the dust clusters after applying the electric field is smaller when fitted to the stellar spectrum. It is about [1–4.3] times the size of the dust cluster without the electric field and considering the ionized state.

Acknowledgments

We would like to thank Professor Zhanwen Han and Professor Zhengwei Liu of Yunnan Astronomical Observatory of the Chinese Academy of Sciences, and Professor Aigen Li of the University of Missouri for their help. Besides, we are grateful for resources from the High-Performance Computing Center of Central South University. This work has also received substantial support from these projects, mainly including the Independent Innovation Project for Postgraduates of Central South University (No. 160171008), the National Natural Science Foundation of China (project No. U2031204), and the project of Xinjiang (No. 2021D01C075).

References

- Abplanalp, M. J., & Kaiser, R. I. 2020, *ApJ*, **889**, 3
- Allamandola, L. J., Tielens, A. G. G. M., & Barker, J. R. 1989, *ApJS*, **71**, 733
- An, J. H., & Sellgren, K. 2003, *ApJ*, **599**, 312
- Andrews, H., Candian, A., & Tielens, A. G. G. M. 2016, *A&A*, **595**, A23
- Babich, L. P., Bochkov, E. I., & Kutsyk, I. M. 2007, *Ge&Ae*, **47**, 671
- Beltrán, M. T., Cesaroni, R., Rivilla, V. M., et al. 2018, *A&A*, **615**, A141
- Bond, A. D. 2010, *Acta Cryst.*, **66**, o2768
- Bouchouit, K., Bendheif, L., & Cherif, N. B. 2004, *AcCrE*, **60**, o272
- Brandl, B. R., Bernard-Salas, J., Spoon, H. W. W., et al. 2006, *ApJ*, **653**, 1129
- Brar, V., Sherrott, M., Jang, M., et al. 2015, *NatCo*, **6**, 7032
- Cecchi-Pestellini, C., Mallocci, G., Mulas, G., Joblin, C., & Williams, D. A. 2008, *A&A*, **486**, L25
- Cinquegrana, G. C., & Karakas, A. I. 2022, *MNRAS*, **510**, 1557
- Dartois, E., Chabot, M., Pino, T., et al. 2017, *A&A*, **599**, A130
- Draine, B. T. 2003, *ARA&A*, **41**, 241
- Draine, B. T. 2011, in *Physics of the Interstellar and Intergalactic Medium*, ed. J. N. Bahcall & J. P. Ostriker (Princeton, NJ: Princeton Univ. Press), 567
- Draine, B. T., Li, A., Hensley, B. S., et al. 2021, *ApJ*, **917**, 3
- Duley, W. 1976, *Natur*, **263**, 485
- Duolikhun, A., Zhu, C., Wang, Z., et al. 2019, *PASP*, **131**, 124202
- Fan, D., Chen, C., Lu, S., et al. 2020, *ACS Appl. Mater. Interfaces*, **12**, 30297
- Ferland, G. J., et al. 2017, *RMxAA*, **53**, 385
- Ferrarotti, A. S., & Gail, H. P. 2006, *A&A*, **447**, 553
- Genzel, R., Lutz, D., Sturm, E., et al. 1998, *ApJ*, **498**, 579
- Glatzle, M., Graziani, L., & Ciardi, B. 2022, *MNRAS*, **510**, 1068
- Haley, M. M., Bell, M. L., & English, J. J. 1997, *JChS*, **119**, 2957
- Hanine, M., Meng, Z., Lu, S., et al. 2020, *ApJ*, **900**, 188
- Hossain, M. S., Rahaman, S. A., Hatai, J., Saha, M., & Bandyopadhyay, S. 2020, *ChCom*, **56**, 2317
- Ivlev, A. V., Padovani, M., Galli, D., & Caselli, P. 2015, *ApJ*, **812**, 135
- Jagannathan, S., Sharma, R., & Seshadri, T. R. 2021, *IJMPD*, **30**, 1
- Joham, H., & Dorfi, E. A. 2012, *A&A*, **541**, A107
- Karakas, A. I., & Lattanzio, J. C. 2007, *PASA*, **24**, 103
- Kirchhoff, G. R. 1860, *AnP*, **185**, 275
- Kohn, W., & Sham, L. J. 1965, *PhRv*, **140A**, 1133
- Lacy, J. H., Evans, N. J., Achtermann, J. M., et al. 1989, *ApJL*, **342**, L43
- Lattanzi, V., Gottlieb, C. A., Thaddeus, P., Thorwirth, S., & McCarthy, M. C. 2015, in *AIP Conf. Ser. 1642, Computational Methods in Sciences and Engineering 2010 (ICCMSE-2010)* (Melville, NY: AIP), 358
- Li, A. 2020, *NatAs*, **4**, 339
- Li, Y., Liao, Y., & Chen, Z. 2014, *Angew. Chem., Int. Ed.*, **53**, 7248
- Lin, L., Li, X., Zhang, B., Zhang, Z., & He, M. 2016, *CJIC*, **32**, 1653
- Mallocci, G., Mulas, G., Cecchi-Pestellini, C., & Joblin, C. 2008, *A&A*, **489**, 1183
- Marassi, S., Schneider, R., Limongi, M., et al. 2019, *MNRAS*, **484**, 2587
- Marciniak, A., Despré, V., Barillot, T., et al. 2015, *NatCo*, **6**, 7909
- McCarthy, M. C., Chen, W., Travers, M. J., & Thaddeus, P. 2000, *ApJ*, **129**, 611
- McMullan, R. K., Kvik, Å., & Popelier, P. 1992, *Acta Cryst.*, **48**, 726
- Murga, M. S., Wiebe, D. S., Sivkova, E. E., & Akimkin, V. V. 2019, *MNRAS*, **488**, 965
- Nagasaka, S., Miyakawa, M., Usugi, T., & Takahashi, Y. 2005, *JPSJ*, **74**, 6
- Neugebauer, J., & Scheffler, M. 1992, *PhRvB*, **46**, 16067
- Orszagh, J., Ribar, A., Danko, M., et al. 2022, *ChemPhysChem*, **23**, 2
- Paul, A., & Grinberg, I. 2022, *PhRvP*, **17**, 024042
- Peeters, E., Allamandola, L. J., Hudgins, D. M., Hony, S., & Tielens, A. G. G. M. 2004, in *ASP Conf. Ser. 309, Astrophysics of Dust*, ed. A. N. Witt, G. C. Clayton, & B. T. Draine (San Francisco, CA: ASP), 141
- Pereira, R. C., de Barros, A. L. F., da Costa, C. A. P., et al. 2020, *MNRAS*, **495**, 40
- Porter, T. A., Jóhannesson, G., & Moskalenko, I. V. 2017, *ApJ*, **846**, 1
- Rani, P., Dubey, G. S., & Jindal, V. K. 2014, *PHYSICA E*, **62**, 28
- Rho, J., Evans, A., Geballe, T. R., et al. 2021, *ApJ*, **908**, 232
- Sales, D. A., Pastoriza, M. G., & Riffel, R. 2010, *ApJ*, **725**, 605
- Sarang, A., Dwek, E., & Arendt, R. G. 2018, *ApJ*, **859**, 66
- Sellgren, K. 1984, *ApJ*, **277**, 623
- Siebenmorgen, R., Voshchinnikov, N. V., & Bagnulo, S. 2014, *A&A*, **561**, A82
- Silva-Ribeiro, A., Krabbe, A. C., Canelo, C. M., et al. 2022, *MNRAS*, **509**, 327
- Smith, J. D. T., Draine, B. T., Dale, D. A., et al. 2007, *ApJ*, **656**, 770
- Sukhinin, G. I., Fedoseev, A. V., Khokhlov, R. O., & Suslov, S. Yu. 2012, *CoPP*, **52**, 62
- Takahashi, O., Yamamura, R., Tokushima, T., & Harada, Y. 2022, *PhRvL*, **128**, 086002
- Tang, D., Xu, Y. Z., Wang, W. W., et al. 2019, *J. Nat. Prod.*, **82**, 1599
- Tazaki, R., Ichikawa, K., & Kokubo, M. 2020, *ApJ*, **892**, 84
- Tielens, A. G. G. M. 2005, in *The Physics and Chemistry of the Interstellar Medium*, ed. A. G. G. M. Tielens (Cambridge: Cambridge Univ. Press)
- Tielens, A. G. G. M. 2008, *ARA&A*, **46**, 289
- Todini, P., & Ferrara, A. 2001, *MNRAS*, **325**, 726
- van Broekhuizen, F. A., Keane, J. V., & Schutte, W. A. 2004, *A&A*, **415**, 425
- van Hoof, P. A. M., Van de Steene, G. C., et al. 2020, *CAOSP*, **50**, 32
- Ventura, P., Dell’Aglia, F., Lugaro, M., et al. 2020, *A&A*, **641**, A103
- Ventura, P., Dell’Aglia, F., Romano, D., et al. 2021, *A&A*, **655**, A6
- Wang, Y., Li, F., Li, Y., & Chen, Z. 2016, *NatCo*, **7**, 11488
- Waxman, E., & Draine, B. T. 2000, *ApJ*, **537**, 796
- Wenzel, G., Joblin, C., Giuliani, A., et al. 2020, *A&A*, **641**, A98
- Worsham, J. E., Levy, H. A., & Peterson, S. W. 1957, *AcCr*, **10**, 323
- Wu, R.-Q., Long, M.-Q., Zhang, X.-J., et al. 2022, *RAA*, **22**, 035014
- Wu, R.-Q., Zhu, C.-H., Lü, G.-L., Wang, Z.-J., & Liu, H.-L. 2021, *RAA*, **21**, 129
- Yamagishi, M., Kaneda, H., Ishihara, D., et al. 2012, *A&A*, **541**, A10
- Yao, M. L., Zhang, X. J., Wu, T., et al. 2021, *JAP*, **129**, 035302
- Yin, J. L., Pulisiano, A., & Palmer, R. E. 2006, *SMALL*, **2**, 744
- Yin, Z. B., Chen, X. Y., & Long, M. Q. 2022, *JPCM*, **34**, 3
- Zhang, S., Zhang, X., Li, M., et al. 2018, *PhLA*, **382**, 2769
- Zhen, J., Rodriguez Castillo, S., Joblin, C., et al. 2016, *ApJ*, **822**, 113
- Zhu, C., Liu, H., Lü, G., Wang, Z., & Li, L. 2019, *MNRAS*, **488**, 525
- Zhu, C., Lü, G., Wang, Z., & Liu, J. 2013, *PASP*, **125**, 25